Numerical simulation of double-diffusive mixed convection and entropy generation in a lid-driven trapezoidal enclosure with a heat source

Ahmad Ababaei[a], Mahmoud Abbaszadeh[b,*], Ali Arefmanesh[a], Ali J. Chamkha[c,d]

[a] Department of Mechanical Engineering, University of Kashan, Kashan, Iran (Postal Code: 8731753153)

[b] School of Engineering, University of Warwick, Coventry CV4 7AL, United Kingdom

[c] Mechanical Engineering Department, Prince Sultan Endowment for Energy and Environment, Prince Mohammad Bin Fahd University, Al-Khobar 31952, Saudi Arabia

[d] RAK Research and Innovation Center, American University of Ras Al Khaimah, P.O. Box 10021, Ras Al Khaimah, United Arab Emirates

Abstract

In this study, entropy generation of double-diffusive mixed convection is investigated inside a right-angled trapezoidal cavity with a partially heated and salted bottom wall. Similar to the approach that assigns color to streamlines, a new coloring scheme is employed to visualize heatlines and masslines in a more meaningful manner. In addition, various consequential parameters, namely the Lewis and Richardson numbers, the buoyancy ratio, the direction of lid movement, and the heat source location, have been analyzed. According to the results, as the Lewis number increases, the average Nusselt number declines, while the total entropy generation augments. Furthermore, for Le = 0.1, the conduction mass transfer dominates the mass transfer field; hence, the masslines are virtually perpendicular to the isoconcentration lines.

Keywords: Colored heatlines and masslines; Double-diffusive mixed convection; Heat and mass transfer; Entropy generation.

[*]Corresponding author
E-mail address: m.abbaszadeh@warwick.ac.uk (M. Abbaszadeh).

Nomenclature

Be	Bejan number
Br	buoyancy ratio
c	species concentration (kg m^{-3})
C	dimensionless species concentration
D	mass diffusivity (m^2 s^{-1})
Gr	Grashof number
g	gravitational acceleration (m s^{-2})
H	dimensionless heatfunction
k	thermal conductivity (W m^{-1} K^{-1})
L	enclosure length (m)
L_h	heat source distance from origin (m)
Le	Lewis number
M	dimensionless massfunction
n	unit normal vector
Nu	Nusselt number
p	pressure (N m^{-2})
P	dimensionless pressure
Pr	Prandtl number
R	gas constant (= 8.314 J mol^{-1} K^{-1})
Re	Reynolds number
Ri	Richardson number
$\dot{s}'''$	volumetric rate of entropy generation (W m^{-3} K^{-1})
$\dot{S}'''$	dimensionless volumetric rate of entropy generation
$\dot{S}$	dimensionless overall rate of entropy generation
Sh	Sherwood number
T	temperature (K)
(u,v)	velocity components (m s^{-1})

(U, V)	dimensionless velocity components
(x, y)	coordinates (m)
(X, Y)	dimensionless coordinates
Greek symbols	
α	thermal diffusivity ($m^2\ s^{-1}$)
β_c	coefficient of solutal expansion ($m^3\ kg^{-1}$)
β_T	coefficient of thermal expansion (K^{-1})
γ	Angle between inclined and bottom wall
θ	dimensionless temperature
μ	dynamic viscosity ($kg\ m^{-1}\ s^{-1}$)
ν	kinematic viscosity ($m^2\ s^{-1}$)
ρ	density ($kg\ m^{-3}$)
ϕ_i	irreversibility distribution ratios
Ψ	dimensionless streamfunction
Ω	computational domain
Subscripts	
0	reference state
av	average or mean
c	cold
h	hot or high
l	low
Superscripts	
*	dimensionless

1. Introduction

As far as the world's fossil fuel resources are limited, considerable efforts should be directed into designing devices and processes in engineering systems. Furthermore, in order to attain multi-faceted targets of an engineering system, a creative, iterative, and open-ended process which results in effective thermal and fluid system designing, is required. To satisfy such a need, the Second Law of Thermodynamics should be considered in analyzing a thermal fluid system to promote its energy efficiency. Moreover, the criterion to assess for energy efficiency of engineering devices is entropy generation which plays a significant role in clarifying the maximum theoretical limits of energy efficiency. It is worth mentioning that the thermal, friction, and other thermodynamic irreversibilities, which are responsible for inefficiencies in an engineering thermal fluid system, are taken into account in formulating entropy generation. Numerous studies were dedicated to scrutinize the entropy generation and convection heat transfer in enclosures over the past few years [1-11]. Baytas [12] conducted a numerical simulation to study entropy generation and natural convection heat transfer in an inclined square cavity. He observed that in low Rayleigh numbers that the effects of heat transfer irreversibility are more than fluid friction irreversibility. Natural convection heat transfer and entropy generation in a square enclosure is numerically investigated by Mahmud and Fraser [13]. Based on their results, the entropy generation in the center of the enclosure is lower in magnitude compared to near the cavity walls. In another numerical investigation, Ovando-Chacon et al. [14] examined entropy generation due to mixed convection heat transfer in a square cavity. They observed that the high entropy generation due to fluid friction irreversibility occurs near the vertical moving walls; and the minimum and maximum entropy generation due to heat transfer irreversibility takes place on the middle of the cavity walls and in the zones with large temperature gradients, respectively. Moreover, they demonstrated that when the Richardson number increases, the heat transfer irreversibility near the boundaries of the cavity increases. Khorasanizadeh et al. [15] utilized the finite volume method and the SIMPLER algorithm to explore mixed convection and entropy generation in a lid-driven square cavity. Based upon their results, when the Reynolds number increases, both terms of entropy generation augment; and as the Rayleigh number increases, the heat transfer term of entropy generation increases and entropy generation due to fluid friction decreases. They also demonstrated that the maximum

entropy generation is for low Rayleigh and high Reynolds numbers, and the minimum entropy generation appertains to low Rayleigh and low Reynolds numbers. Very recently, Nayak et al. [16] conducted a numerical investigation to explore mixed convection heat transfer and entropy generation in a lid-driven square enclosure. The results have shown that the entropy is generated mainly because of heat transfer irreversibility. They also concluded that the Bejan number increases as the Reynolds number increases at a constant Grashof number, but it decreases with increase of the Grashof number when the Reynolds number is constant. Mixed convective heat transfer of nanofluid and its entropy generation in a trapezoidal cavity is examined by Aghaei et al. [17]. They observed that in all of considered cases, the entropy generation due to fluid friction is negligible and entropy virtually generated due to heat transfer. They also showed that in Reynolds number of 1000, moving direction of the lid does not have profound effects on the total entropy generation and the average Nusselt number, but in Reynolds number of 30 this behavior is completely reversed.

When the buoyancy forces take place as a result of temperature and concentration gradients, the concept of double-diffusive natural convection appears. In other word, in order to calculate the density of a fluid, the effects of the temperature gradients and concentration gradients should be taken into account simultaneously. Double-diffusive natural convection has been encountered in different ranges of natural systems such as atmosphere, ocean circulation, asthenosphere movement within crust, pollution transportation in air, astrophysics, geology, biology, chemical processes, etc. The debate surrounding double-diffusive convection has witnessed many controversies in the last three decades [18-24]. As early as 1987, Trevisan and Bejan [25] numerically and analytically examined natural convection heat transfer due to the buoyancy effects of both temperature and concentration in a rectangular slot subjecting to uniform heat and mass fluxes. Double-diffusive natural convection of moist air flowing inside a square cavity with heat and mass diffusive walls is investigated by Costa [26] using the SIMPLER algorithm based on finite volume method. They obtained that buoyancy ratio has a great impact on both the temperature and concentration fields, parameters of both heat and mass transfer fields as well as the routes tracked by the heat and mass streams. Al-Amiri et al. [27] conducted a numerical simulation to study mixed convection heat transfer in a lid-driven square enclosure under the buoyancy effects of both thermal as well as solutal diffusion. Based on their results, characteristics of heat and mass transfer within the cavity are enhanced for low Richardson

numbers due to the moving lid. Moreover, they observed that Lewis number has not far-reaching effect on the isotherms and streamlines in small Richardson numbers. In another numerical investigation, Hasanuzzaman et al. [28] analyzed double-diffusive mixed convection in a right triangular enclosure occupied with air. They showed that as the Lewis number increases, heat transfer decreases for all studied parameters. They also demonstrated that when the Lewis number augments, the Sherwood number increases almost linearly; also, higher Sherwood numbers appertain to higher values of Richardson numbers. Oueslati et al. [29] carried out a numerical study to explore entropy generation of double-diffusive natural convection inside a rectangular enclosure with partial, vertical, thermal and solutal sources. They observed that by increasing the Lewis number, the heat and mass transfer rates significantly increases. They also concluded that the entropy generation is low within the enclosure with the exception of the vicinity of the active vertical walls, especially in the zones where there are high velocity gradients. Qin et al. [30] numerically investigated double-diffusive convection of a binary mixed fluid in a rectangular enclosure with horizontal temperature and concentration gradients. Their results showed that the Sherwood number increases with the Lewis number. Very recently, Arbin et al. [31] numerically studied double-diffusive natural convection in an open top square cavity via the heatlines approach. According to their findings, higher values of Lewis number will decrease the heat transfer rates, but will enhance the mass transfer rates. Teamah et al. [32] numerically investigated the double-diffusive natural convection in the presence of magnetic field inside a trapezoidal cavity. The results showed that heat and mass transfer rates decline when the Hartmann number increases.

In order to gain a better physical insight about heat and mass transfer in enclosures, the heatlines and masslines visualization techniques have been proposed as innovative approaches which pave the way. In order to visualize how the energy flows through the convective heat transfer fields, heatlines were presented and used for the first time by Kimura and Bejan [33]. Subsequently, masslines were put forward by Trevisan and Bejan [25] in order to visualize convective mass transfer fields. Then, Costa [34] presented a thorough survey on the use of heatlines and masslines. As a glance at aforementioned literature, and even the new studies where heatlines and masslines visualization techniques are used [35-37], it is incontrovertibility axiomatic that the coloring scheme is not applied in most of the studies. Moreover, in only a few studies [31, 38] in which heatlines and masslines are presented in color, the colors are not

meaningful. Therefore, in this study, heatlines, masslines, and streamlines are colored in a way that there is a quite clear-cut distinction between the zones where the momentum, heat, and mass transfer are higher and those where the momentum, heat, and mass transfer are lower.

As evidenced by immense, well-documented, and proliferation literature pertaining to double-diffusive convection, it is crystal clear that there has been a little focus on entropy generation of double-diffusive mixed convection inside a trapezoidal cavity and an in-depth analysis about it remains to be addressed. Also, the colored heatlines and masslines technique have never been used in any of these studies. Hence, in this study, double-diffusive mixed convection heat transfer and entropy generation in a trapezoidal enclosure is examined. The set of equations associated with this problem are numerically solved by employing the well-known SIMPLER algorithm. The convective heat and mass transfer fields are depicted using colored heatlines and masslines. The effects of different parameters such as the Lewis number, buoyancy ratio, Richardson number, direction of lid movement and the heat source location are discussed and assessed, and the implications of using these parameters on heat and mass transfer as well as entropy generation are investigated.

2. Physical model and formulation

2.1.Physical model and governing equations

The shape of the cavity is displayed in Fig. 1. It has a height of $0.5L$ and its lower wall has length L. The enclosure's inclined wall is kept at low temperature and low concentration T_c and c_l, respectively. Moreover, the partially heated and salted lower wall is maintained at constant temperature and concentration T_h and c_h, respectively. The heat and mass sources are coincident. The remaining walls of the cavity are insulated and impermeable. The top wall moves from right to left and vice versa with a constant speed u_0. The incompressible fluid is presumed to be Newtonian. All of the thermo-physical properties of the fluid are considered to be constant except for the density variations in the buoyancy terms where the Boussinesq approximation is applied as follows:

$$\rho = \rho_0 \left[1 - \beta_T \left(T - T_c \right) + \beta_c \left(c - c_1 \right) \right], \tag{1}$$

where ρ_0 is the fluid density at the reference temperature and concentration of $T_0 = (T_h + T_c)/2$ and $c_0 = (c_h + c_l)/2$, respectively. $\beta_T = -(1/\rho_0)(\partial\rho/\partial T)_c$ and $\beta_c = -(1/\rho_0)(\partial\rho/\partial c)_T$ are the thermal and solutal expansion coefficients, respectively.

The balance equations of mass, momentum, energy, and species concentration for the steady, laminar, two-dimensional mixed convection fluid flow and heat and mass transfer are as follows:

$$\frac{\partial u}{\partial x} + \frac{\partial v}{\partial y} = 0 \ , \tag{2}$$

$$u\frac{\partial u}{\partial x} + v\frac{\partial u}{\partial y} = -\frac{1}{\rho}\frac{\partial p}{\partial x} + \nu\left(\frac{\partial^2 u}{\partial x^2} + \frac{\partial^2 u}{\partial y^2}\right), \tag{3}$$

$$u\frac{\partial v}{\partial x} + v\frac{\partial v}{\partial y} = -\frac{1}{\rho}\frac{\partial p}{\partial y} + \nu\left(\frac{\partial^2 v}{\partial x^2} + \frac{\partial^2 v}{\partial y^2}\right) + g\left[\beta_T (T - T_c) + \beta_c (c - c_l)\right] \ , \tag{4}$$

$$u\frac{\partial T}{\partial x} + v\frac{\partial T}{\partial y} = \alpha\left(\frac{\partial^2 T}{\partial x^2} + \frac{\partial^2 T}{\partial y^2}\right) \ , \tag{5}$$

and

$$u\frac{\partial c}{\partial x} + v\frac{\partial c}{\partial y} = D\left(\frac{\partial^2 c}{\partial x^2} + \frac{\partial^2 c}{\partial y^2}\right), \tag{6}$$

where u and v are the velocity components in the x and y directions, respectively. ρ and ν are the fluid density and the kinematic viscosity, respectively. Moreover, T, p, c, g, α , and D are the temperature, the pressure, the concentration, the gravitational acceleration, the thermal diffusivity, and the mass diffusivity, respectively.

The volumetric rate of generated entropy [39], assuming that the fluid behaves as a binary perfect gas mixture [40], can be calculated as follows:

$$\begin{aligned} \dot{S}''' = {} & \frac{k}{T_0^2}\left[\left(\frac{\partial T}{\partial x}\right)^2 + \left(\frac{\partial T}{\partial y}\right)^2\right] + \frac{\mu}{T_0}\left[2\left\{\left(\frac{\partial u}{\partial x}\right)^2 + \left(\frac{\partial v}{\partial y}\right)^2\right\} + \left(\frac{\partial u}{\partial y} + \frac{\partial v}{\partial x}\right)^2\right] \\ & + \frac{RD}{c_0}\left[\left(\frac{\partial c}{\partial x}\right)^2 + \left(\frac{\partial c}{\partial y}\right)^2\right] + \frac{RD}{T_0}\left[\left(\frac{\partial T}{\partial x}\right)\left(\frac{\partial c}{\partial x}\right) + \left(\frac{\partial T}{\partial y}\right)\left(\frac{\partial c}{\partial y}\right)\right], \end{aligned} \tag{7}$$

where R is the gas constant which is equal to 8.314 J/mol K.

The set of Eqs. (2)–(6) can be changed to their dimensionless forms by replacing the main parameters with their corresponding dimensionless variables that are given below:

$$(X,Y)=\frac{(x,y)}{L},\ (U,V)=\frac{(u,v)}{u_0},\ P=\frac{p}{\rho u_0},\ \theta=\frac{T-T_c}{\Delta T},\ C=\frac{c-c_l}{\Delta c}, \tag{8}$$

where $\Delta T=T_h-T_c$ and $\Delta c=c_h-c_l$. Using the foregoing dimensionless variables, the dimensionless form of the governing equations is written as:

$$\frac{\partial U}{\partial X}+\frac{\partial V}{\partial Y}=0, \tag{9}$$

$$U\frac{\partial U}{\partial X}+V\frac{\partial U}{\partial Y}=-\frac{\partial P}{\partial X}+\frac{1}{\mathrm{Re}}\left(\frac{\partial^2 U}{\partial X^2}+\frac{\partial^2 V}{\partial Y^2}\right), \tag{10}$$

$$U\frac{\partial U}{\partial X}+V\frac{\partial U}{\partial Y}=-\frac{\partial P}{\partial X}+\frac{1}{\mathrm{Re}}\left(\frac{\partial^2 U}{\partial X^2}+\frac{\partial^2 V}{\partial Y^2}\right)+\mathrm{Ri}(\theta+\mathrm{Br}C), \tag{11}$$

$$U\frac{\partial \theta}{\partial X}+V\frac{\partial \theta}{\partial Y}=\frac{1}{\mathrm{RePr}}\left(\frac{\partial^2 \theta}{\partial X^2}+\frac{\partial^2 \theta}{\partial Y^2}\right), \tag{12}$$

and

$$U\frac{\partial C}{\partial X}+V\frac{\partial C}{\partial Y}=\frac{1}{\mathrm{RePrLe}}\left(\frac{\partial^2 C}{\partial X^2}+\frac{\partial^2 C}{\partial Y^2}\right), \tag{13}$$

where the Reynolds, Prandtl, Lewis, Grashof and Richardson numbers, and the buoyancy ratio are defined, respectively, as

$$\mathrm{Re}=\frac{u_0 L}{\nu},\ \mathrm{Pr}=\frac{\nu}{\alpha},\ \mathrm{Le}=\frac{\alpha}{D},\ \mathrm{Gr}=\frac{g\beta_T \Delta T L^3}{\nu^2},\ \mathrm{Ri}=\frac{\mathrm{Gr}}{\mathrm{Re}^2},\ \mathrm{Br}=\frac{\beta_c \Delta c}{\beta_T \Delta T} \tag{14}$$

The Prandtl and Grashof numbers, which are considered to be constant in this study, are equal to $\mathrm{Pr}=0.71$ and $\mathrm{Gr}=10^4$, respectively.

The dimensionless volumetric rate of entropy generation is given by:

$$S''' = S'''\frac{L^2 T_0^{\,2}}{k\,\Delta T^{\,2}} = \left[\left(\frac{\partial\theta}{\partial X}\right)^2 + \left(\frac{\partial C}{\partial Y}\right)^2\right] + \phi_1\left[2\left\{\left(\frac{\partial U}{\partial X}\right)^2 + \left(\frac{\partial V}{\partial Y}\right)^2\right\} + \left(\frac{\partial U}{\partial Y} + \frac{\partial V}{\partial X}\right)^2\right] + \phi_2\left[\left(\frac{\partial C}{\partial X}\right)^2 + \left(\frac{\partial C}{\partial Y}\right)^2\right] + \phi_3\left[\left(\frac{\partial\theta}{\partial X}\right)\left(\frac{\partial C}{\partial X}\right) + \left(\frac{\partial\theta}{\partial Y}\right)\left(\frac{\partial C}{\partial Y}\right)\right], \tag{15}$$

where ϕ_1, ϕ_2 and ϕ_3 ,which denote the irreversibility distribution ratios, are defined as follows:

$$\phi_1 = \frac{\mu T_0}{k}\left(\frac{u_0}{\Delta T}\right)^2, \quad \phi_2 = \frac{RD}{kc_0}\left(T_0\frac{\Delta c}{\Delta T}\right)^2, \quad \phi_3 = \frac{RD}{k}\left(T_0\frac{\Delta c}{\Delta T}\right) \tag{16}$$

It is to be noted that these irreversibility distribution ratios are assumed constant and equal to $\phi_1 = 10^{-4}$, $\phi_1 = 0.5$ and $\phi_1 = 10^{-2}$ [29, 40, 41].

The corresponding non-dimensional boundary conditions for Eqs. (9)–(13) are as follows:

$U = V = 0$, and $\theta = C = 1$ on the sources,

$U = V = 0$, and $\theta = C = 0$ at the inclined wall,

$U = \pm 1,\ V = 0$, and $\dfrac{\partial\theta}{\partial n} = \dfrac{\partial C}{\partial n} = 0$ at the top wall, (17)

$U = V = \dfrac{\partial\theta}{\partial n} = \dfrac{\partial C}{\partial n} = 0$ along the remaining walls.

The overall rate of entropy produced by the irreversibilities can be calculated by integrating the volumetric rate of irreversibilities over the entire domain as follows:

$$S = \int_\Omega S'''\,d\Omega \tag{18}$$

The average Nusselt and Sherwood numbers along the heat and mass source on the bottom wall are evaluated from the following equations:

$$\mathrm{Nu}_{\mathrm{av}} = \frac{1}{0.5}\int_{L_h^*}^{L_h^*+0.5} -\left.\frac{\partial\theta}{\partial Y}\right|_{Y=0} dX\ , \tag{19}$$

and

$$\mathrm{Sh}_{\mathrm{av}} = \frac{1}{0.5}\int_{L_h^*}^{L_h^*+0.5} -\left.\frac{\partial C}{\partial Y}\right|_{Y=0} dX\ , \tag{20}$$

where $L_h^* = L_h / L$.

2.2.Visualization Method

In this study, the integration method [42] is employed to visualize streamlines, heatlines, and masslines. Moreover, a new coloring approach is also used for the purpose of illustrating heatlines and masslines in a more meaningful manner. This approach is going to be discussed later in this section.

Initially, a bird's-eye view of the entire flow field and its main characteristics are demonstrated by means of the streamfunction, which is obtained from the conservation of mass equation. The streamfunction values can be calculated from:

$$\Psi(X,Y) = \Psi(X,0) + \int_{(X,0)}^{(X,Y)} U dY \ , \tag{21}$$

where $\Psi_0 = \Psi(0,0)$ is randomly set to zero; therefore, $\Psi(X,0) = \Psi_0 = 0$, because $\partial\Psi/\partial X\big|_{Y=0} = -V(X,0) = 0$.

The conservation of energy equation can be rearranged and, similar to the streamfunction, the heatfunction can be defined as:

$$\frac{\partial H}{\partial Y} = U\theta - \alpha^* \frac{\partial \theta}{\partial X}, \text{and } -\frac{\partial H}{\partial X} = V\theta - \alpha^* \frac{\partial \theta}{\partial Y}, \tag{22}$$

where $\alpha^* = 1/\mathrm{Re}\,\mathrm{Pr}$. Obviously, the heatfunction is able to satisfy the conservation of energy equation. It represents the local strength of the convective heat transfer, which is composed of the advective heat fluxes $(U\theta, V\theta)$ as well as the conductive or diffusive heat fluxes $(-\partial\theta/\partial X, -\partial\theta/\partial Y)$. In order to visualize the heatlines, the heatfunction quantities are obtained by integrating Eq. (22) as follows:

$$H(X,0) = H(0,0) + \int_{(0,0)}^{(X,0)} \left(\alpha^* \frac{\partial \theta}{\partial Y} - V\theta \right) dX \ , \tag{23}$$

and

$$H(X,Y) = H(X,0) + \int_{(X,0)}^{(X,Y)} \left(U\theta - \alpha^* \frac{\partial \theta}{\partial X} \right) dY \ , \tag{24}$$

where $H_0 = H(0,0) = 0$.

A similar conclusion can be drawn after the conservation of species concentration equation is rearranged:

$$\frac{\partial M}{\partial Y} = UC - D^* \frac{\partial C}{\partial X}, \text{and } -\frac{\partial M}{\partial X} = VC - D^* \frac{\partial C}{\partial Y}, \tag{24}$$

where $D^* = 1/\mathrm{Re}\,\mathrm{Pr}\mathrm{Le}$. The massfunction values, which consist of advective and conductive mass fluxes, is calculated by integrating (24) as follows:

$$M(X,0) = M(0,0) + \int_{(0,0)}^{(X,0)} \left(D^* \frac{\partial C}{\partial Y} - VC \right) dX, \tag{25}$$

and

$$M(X,Y) = M(X,0) + \int_{(X,0)}^{(X,Y)} \left(UC - D^* \frac{\partial C}{\partial X} \right) dY, \tag{26}$$

where $M_0 = M(0,0) = 0$.

The mentioned coloring approach presents the heatlines and masslines in a way that is both meaningful and easier to interpret. This is analogous to the coloring of streamlines when they are colored by absolute values of velocity (i.e. $\sqrt{u^2 + v^2}$). Thus, absolute convective values of heatlines and masslines are applied as coloring on the lines. In other words, streamlines, heatlines, and masslines are colored in each point with values of $\sqrt{U^2 + V^2}$, $\sqrt{(\partial H/\partial X)^2 + (\partial H/\partial Y)^2}$, and $\sqrt{(\partial M/\partial X)^2 + (\partial M/\partial Y)^2}$, respectively. As a result, the coloration of heatlines and masslines shows the local intensity of energy or mass transfer rate in the heat or mass transfer field. Hence, it becomes easier to appreciate and analyze these fields.

3. Numerical implementation

By using the finite volume method [43], a FORTRAN code is developed in order to solve the governing equations. The code was based on the SIMPLER algorithm [44], which is able to

handle the coupling between the pressure and velocities. The diffusive and advective terms in Eqs. (10)–(13) are discretized by employing the power-law differencing scheme, and the corresponding set of discretized equations are solved using a TDMA line-by-line solver.

3.1.Benchmarking of the code

The correct modeling of the code is verified by developing a similar code to simulate the existing results of other studies. The geometries as well as the boundary conditions of the considered test cases are illustrated in Fig. 2. Comparisons between the heat transfer, the fluid friction irreversibilities, the total rate of entropy generation, and the local Bejan number of the present study code with those of Ilis et al. [45] are shown in Fig. 3 for Pr = 0.7 in Ra = 10^5. Moreover, Fig. 4 shows comparisons between the isotherms and the isoconcentration lines in the square enclosure using the developed code with the results of Al-Amiri et al. [27]. The results in this figure are for Pr = 1, Ri = 0.01, Re = 100, Br = 1 and Le = 5 and 50. Figs. 3 and 4 exhibit a sufficiently good agreement between the simulated results of the present code and those of Al-Amiri et al. [27] and Ilis et al. [45], thereby guaranteeing the accuracy of the findings acquired by the present study.

3.2.Finding an independent grid

To find a proper grid for the numerical simulations, a test of grid independency is conducted for the mixed convection flow at Ri = 100, Le = 10, Br = -10, and γ = 45°. The obtained average Nusselt number and the total entropy generation for different girds are presented in Table 1. As evidenced by this table, when the grid 201×101 is replaced with the grid 301×151, the maximum relative difference between the two grid systems becomes 1.68%, which is clearly a negligible change. Therefore, the grid system having 201×101 nodes is a proper grid for simulations and it is applied to the subsequent numerical calculation. All of the following results are obtained employing this grid.

4. Results and discussion

The entropy generation of double-diffusive mixed convection is examined in a right-angled trapezoidal cavity that is partially heated and salted. The effects of different parameters such as the Lewis number, the buoyancy ratio, the Richardson number, the direction of the lid movement

and the heat source location on the flow and temperature fields are studied. The study is conducted for $0.01 < Ri < 100$, $-10 < Br < 10$, $0.1 < Le < 10$, $Pr = 0.7$, $Gr = 10^4$, and $\gamma = 45°$ and 60°.

4.1. Isotherms, isoconcentration lines, streamlines, heatlines, masslines, and constant entropy generation lines

Fig. 5 displays the isotherms, the isoconcentration lines, the streamlines, the heatlines, the masslines, and the constant entropy generation lines for Le = 10, Br = 1, Ri = 0.1 and 10, $\gamma = 45°$ and 60°, and for the two directions of the lid movement. As can be seen from this figure, when the lid moves toward the right side, the clockwise vortex draws the isotherm and the isoconcentration lines from the cold wall toward the heat source, and accumulates them on the heat source. Furthermore, the isotherm and isoconcentration lines are less compressed on the heat source for $\gamma = 60^o$ compared to when $\gamma = 45^o$ due to the fact that for $\gamma = 60^o$, the distance between the cold wall and heat source is more compared to when $\gamma = 45^o$. Moreover, the accumulation of the isotherm and the isoconcentration lines on the hot and the cold boundaries diminish for Ri = 10 compared to when Ri = 0.1 due to the enhanced natural convection strength. A close scrutiny of the streamlines, the heatlines, and the masslines reveals that the velocities have the maximum values near the moving wall. Moreover, the heatlines and the masslines emerge vertically from the heat source and after taking effect from the central vortex, perpendicularly reach to the cold wall. Above the right section of the heat source and upper parts of the cold wall, the heatlines and the masslines have the maximum density implying the maximum rates of heat and mass transfer in these areas, respectively. According to the lines of constant generated entropy, the maximum amount of local generated entropy is seen over the right side of the heat source and upper parts of the cold wall, and the minimum entropy generation takes place on the left bottom corner of the enclosure. Furthermore, when the lid moves toward the left side, the counterclockwise vortex stretches the isotherm and the isoconcentration lines from the heat source toward the cold wall. In this case, a secondary clockwise vortex develops in the right corner of the enclosure which becomes larger with increasing the Richardson number. This vortex alters the layout of the heatlines and the masslines in a way that a second vortex in masslines is formed on that spot. Moreover, according

to the lines of constant generated entropy, the generated entropy in the central part of the heat source decreases in this case.

Fig. 6 illustrates the isotherms, the isoconcentration lines, the streamlines, the heatlines, the masslines, and the constant entropy generation lines for Ri = 1, Br = 4, and γ = 45° and 60° and for different Lewis numbers. As it is observed from the isotherms and the heatlines, variations of the Lewis number does not have a considerable impact on these lines due to the fact that the Lewis number does not affect the energy equation directly. Regarding the isoconcentration lines, increasing the Lewis number compresses the isoconcentration lines, on the high and low concentration walls; while, a region with an average concentration is extended in the central part of the enclosure. Furthermore, high values of the Lewis number signify less mass diffusivity. When the mass diffusivity decreases, the solutal boundary layer becomes thinner and, therefore, the concentration gradient on both high and low salted walls increases resulting in mass transfer enhancement. It is noteworthy that for Le = 1, the diffusion characteristics of heat and mass transfer are identical and as results, the isotherm and isoconcentration lines, as well as the heatlines and the masslines are coincident. Considering the color of streamlines, as the Lewis number increases, the strength of the flow declines, but the structure of the streamlines is maintained. Regarding the masslines, for Le = 0.1, the conduction mass transfer dominates the mass transfer field and so, the masslines are virtually perpendicular to the isoconcentration lines; while by increasing the Lewis number, the masslines are more affected by the primary vortex due to the fact that the conductive mass flux decreases when the Lewis number augments. The constant generated entropy lines show that the entropy generation increases with the Lewis number.

The isotherms, the isoconcentration lines, the streamlines, the heatlines, the masslines, and the constant entropy generation lines for Ri = 100, Le = 0.1, γ = 45° and different buoyancy ratios and heat source locations are shown in Fig. 7. Regarding the isotherms, when $L_h = 0$, the isotherms are drawn from the hot surface toward the cold wall for $\mathrm{Br} = -10$. This behavior is completely reversed for $\mathrm{Br} = 10$ due to the change of the rotating direction of primary vortex from counterclockwise for $\mathrm{Br} = -10$ to clockwise for $\mathrm{Br} = 10$. Moreover, for $\mathrm{Br} = -10$, the downward solutal buoyancy force overwhelmingly dominates the upward thermal buoyancy force changing the direction of the primary vortex. For $\mathrm{Br} = 0$, when the mass transfer has no

effect on flow field, the temperature gradient on the heat source is less than that of the other cases. Regarding the isoconcentration lines, by increasing the buoyancy ratio from -10 to 10, the concentration gradient on the mass source increases. As far as the heatlines and masslines, the heatlines are under the influence of the counterclockwise and clockwise circulations for $\mathrm{Br} = -10$ and $\mathrm{Br} = 10$, respectively. Furthermore, the primary vortex for $\mathrm{Br} = 0$ does not affect the masslines; and the masslines are perpendicular to the isoconcentration lines. This behavior reveals that the conductive mass transfer regime is dominant for Le = 0.1. By considering the constant entropy generation lines, the maximum irreversibility takes place in the right edge of heat source and the upper part of the cold wall. Moreover, for $L_{\mathrm{h}} = 0.25$, as the heat source approaches the cold wall, both of the temperature and concentration gradients increase. According to the constant generated entropy lines, the local generated entropy is maximum at the right side of the heat source. Furthermore, for $L_{\mathrm{h}} = 0.5$, as the heat source approaches toward the cold wall, strong temperature and concentration gradients develop in the right corner of the enclosure. For $\mathrm{Br} = -10$, one primary counterclockwise vortex, accompanied with two secondary clockwise vortices, is formed within the enclosure. For $\mathrm{Br} = 0$, there is just one clockwise vortex, but for $\mathrm{Br} = 10$, one counterclockwise vortex in the left bottom corner of the enclosure is created. Moreover, the heatlines directly reach to the cold wall due to the counterclockwise circulation for $\mathrm{Br} = -10$; whereas for $\mathrm{Br} = 10$, the heatlines initially move toward the center of the enclosure and then, reach to the cold wall. It is worth mentioning that the buoyancy ratio does not affect the masslines significantly; and the maximum entropy generation occurs in the right corner of the enclosure.

4.2.Temperature, concentration and velocity profiles

Fig. 8 displays the variations of the dimensionless temperature, concentration, and velocity along the vertical centerline of the enclosure for γ = 45° and for different buoyancy ratios and Lewis and the Richardson numbers. As can be observed from this figure, by increasing the buoyancy ratio, the temperature in the upper half of the enclosure augments. Moreover, as the Richardson number decreases, the temperature gradients on the top and bottom walls increase and a region with an average temperature develops in the center of the enclosure. Moreover, for $\mathrm{Br} < 0$, the concentration decreases linearly with the height, but for $\mathrm{Br} \geq 0$, the concentration in the upper parts of the enclosure at first increases and then decreases with an increases of the

height. Also, as the Lewis number increases due to diminishing effects of mass diffusion, the concentration gradient on the top and bottom wall augments and a region with an average concentration expands in the center of the enclosure. It should be noted that the variations of the Lewis number does not have significant effect on the velocity profile, and with decreasing the Richardson number, the velocity gradient increases.

4.3.Mean Nusselt and Sherwood numbers, and overall entropy generation

Fig. 9 shows variations of the mean Nusselt and Sherwood numbers and the overall generated entropy with the buoyancy ratio for Ri = 10 and γ = 45° and for different Lewis numbers and two directions of the lid movement. In Figs. 9 a and b, the average Nusselt number decreases when the Lewis number increases. On the other hand, for Le = 0.1 and 1, with augmentation of the buoyancy ratio, the average Nusselt number initially decreases and then increases, because when $|\mathrm{Br}| >> 0$, the buoyancy forces intensify. Furthermore, when $\mathrm{Br} << 0$, the mean Nusselt number is larger when the lid moves toward the left compared to when it moves toward the right. This behavior is reversed for $\mathrm{Br} >> 0$. As it is observed from Figs. 9 c and d, the average Sherwood number decreases as the Lewis number increases. Moreover, with augmentation of the buoyancy ratio, the average Sherwood number initially decreases slightly and then, increases significantly. Similar to the average Nusselt number, for $\mathrm{Br} << 0$, the average Sherwood number is high as the lid moves toward the left compared to when it moves toward the right; whereas, this behavior is reversed for $\mathrm{Br} >> 0$. According to Figs. 9 e and f, with increasing the Lewis number, the entropy generation augments for $\mathrm{Br} >> 0$. Moreover the entropy generation is higher when the lid moves toward the right compared to when it moves toward the left; while, for $\mathrm{Br} << 0$, the minimum entropy generation belongs to Le = 1 and after that to Le = 10 and 0.1; and when the lid moves toward the right side, the entropy generation is less than when the lid moves toward the left side.

Fig. 10 illustrates how the mean Nusselt and Sherwood numbers, and the overall generated entropy change with the Richardson number for Br = 1, Le = 0.1 and 10, and γ = 45° and 60°. Generally, with increasing the Richardson number and decreasing the temperature, the concentration, and the velocity gradients (see Figs. 8 c, f, and i), the mean Nusselt and Sherwood numbers, and the overall generated entropy decrease. Furthermore, the mean Nusselt and Sherwood numbers, and the overall generated entropy for $\gamma = 45^{o}$ are higher than $\gamma = 60^{o}$,

because by decreasing γ, all the gradients increase. Regarding Figs. 10 a and c, when the Lewis number increases, the mean Nusselt number diminishes, while the entropy generation augments. According to Fig. 10 b, for Le = 0.1 when the conduction mass transfer is dominant (see Fig. 6), changing the Richardson number does not have a significant effect on the average Sherwood number.

Variations of the average Nusselt and Sherwood numbers as well as the total entropy generation with the buoyancy ratio are depicted in Fig. 11 for Le = 10, γ = 45° and in different Richardson numbers. According to this figure, by decreasing the Richardson number, the mean Nusselt and Sherwood numbers, and the total generated entropy augment. Also, by reducing the Richardson number and diminishing the buoyancy term in *Y*-momentum equation, the impact of buoyancy ratio on the mean Nusselt and Sherwood numbers as well as the total entropy generation declines. Moreover, for Le = 10, when the buoyancy ratio increases, the mean Nusselt and Sherwood numbers, and the overall generated entropy monotonically increase for $\mathrm{Ri} \geq 1$; while for $\mathrm{Ri} \leq 0.1$, They initially decrease and then augment.

In Fig. 12, variations of the mean Nusselt and Sherwood numbers and the total entropy generation in terms of the Richardson number are displayed for Br = 1, Le = 0.1, γ = 45° and for different locations of the heat source on bottom wall. As can be seen from this figure, for a constant buoyancy ratio, as the Richardson number increases, the average Nusselt and Sherwood numbers, and the total entropy generation decline. Furthermore, as $L_{\mathrm{h}}^{*} = 0.5$, the mean Nusselt and Sherwood numbers, and the total generated entropy drastically increase compared to the other cases. Moreover, changing the Richardson number does not have a meaningful influence on the average Sherwood number for Le = 0.1.

5. Conclusion

In this study, the finite volume method (FVM) is employed in order to study the entropy generation of double-diffusive mixed convection in a right-angled trapezoidal enclosure filled with a binary perfect gas mixture. Also, the convective heat and mass transfer fields are depicted using colored heatlines and masslines, which both proved to be useful tools for interpretation as well as analysis. The effects of the consequential parameters such as the Lewis number, the buoyancy ratio, the Richardson number, the direction of the lid movement and the heat source

location on the heat and mass transfer as well as the entropy generation are examined. Based on the results, the following observations are made:

- The mean Nusselt and Sherwood numbers, and the overall generated entropy for $\gamma = 45^{o}$ are more than those for $\gamma = 60^{o}$ due to the fact that the gradient of the dependent variables increases as γ is reduced.
- For $\mathrm{Br} << 0$, when the lid moves toward the left, the mean Nusselt and Sherwood numbers, and the overall generated entropy are more compared to the case where the lid moves toward the right; while, this behavior is reversed for $\mathrm{Br} >> 0$.
- As the heat source approaches the cold wall, the mean Nusselt and Sherwood numbers, and the overall generated entropy increase, especially for $L_{\mathrm{h}}^{*} = 0.5$ they increase dramatically.
- With the increasing of the Lewis number, the mean Nusselt number decreases, while the entropy generation augments.
- Variation of the Lewis number does not have a considerable impact on the isotherms and the heatlines, but increasing the Lewis number compresses the solutal boundary layer and, therefore, the concentration gradient on both high and low salted walls increases, resulting in mass transfer augmentation.
- For Le = 0.1, the conduction mass transfer dominates the mass transfer field and so, the masslines are virtually perpendicular to the isoconcentration lines. Moreover, the Richardson number does not have a meaningful influence on the average Sherwood number for Le = 0.1.
- With decreasing the Richardson number and the buoyancy term for the *Y*-momentum equation, the impact of the buoyancy ratio on the mean Nusselt and Sherwood numbers as well as the total entropy generation decline. Moreover, for Le = 10, with increasing the buoyancy ratio, the mean Nusselt and Sherwood numbers, and the overall generated entropy monotonically increase for $\mathrm{Ri} \geq 1$; while for $\mathrm{Ri} \leq 0.1$, they initially decrease and then augment.

6. References

[1] A. Bejan, *Entropy generation minimization: the method of thermodynamic optimization of finite-size systems and finite-time processes*: CRC press, 1995.

[2] S. Mahmud and A. S. Islam, Laminar free convection and entropy generation inside an inclined wavy enclosure, *International journal of thermal sciences,* vol. 42, pp. 1003-1012, 2003.

[3] C. Balaji, M. Hölling, and H. Herwig, Entropy generation minimization in turbulent mixed convection flows, *International Communications in Heat and Mass Transfer,* vol. 34, pp. 544-552, 2007.

[4] I. Zahmatkesh, On the importance of thermal boundary conditions in heat transfer and entropy generation for natural convection inside a porous enclosure, *International Journal of Thermal Sciences,* vol. 47, pp. 339-346, 2008.

[5] A. H. Mahmoudi, M. Shahi, and F. Talebi, Entropy generation due to natural convection in a partially open cavity with a thin heat source subjected to a nanofluid, *Numerical Heat Transfer, Part A: Applications,* vol. 61, pp. 283-305, 2012.

[6] M. Esmaeilpour and M. Abdollahzadeh, Free convection and entropy generation of nanofluid inside an enclosure with different patterns of vertical wavy walls, *International Journal of Thermal Sciences,* vol. 52, pp. 127-136, 2012.

[7] A. Bejan, *Convection heat transfer*: John wiley & sons, 2013.

[8] A. Arefmanesh, A. Aghaei, and H. Ehteram, Mixed convection heat transfer in a CuO–water filled trapezoidal enclosure, effects of various constant and variable properties of the nanofluid, *Applied Mathematical Modelling,* vol. 40, pp. 815-831, 2016.

[9] M. Abbaszadeh, A. Ababaei, A. A. Abbasian Arani, and A. A. Sharifabadi, MHD forced convection and entropy generation of CuO-water nanofluid in a microchannel considering slip velocity and temperature jump, *Journal of the Brazilian Society of Mechanical Sciences and Engineering,* vol. 3, pp. 775-790, 2016.

[10] A. Ababaei, M. Abbaszadeh, and A. A. Abbasian Arani, Determining the Optimum Arrangement of Micromixers in a Microchannel Filled with CuO-Water Nanofluid via Minimizing Entropy Generation, in *Defect and Diffusion Forum,* 2017, pp. 39-58.

[11] A. Ababaei, A. A. Abbasian Arani, and A. Aghaei, Numerical Investigation of Forced Convection of Nanofluid Flow in Microchannels: Effect of Adding Micromixer, *Journal of Applied Fluid Mechanics*, vol. 10, pp. 1759-1772, 2017.

[12] A. Baytaş, Entropy generation for natural convection in an inclined porous cavity, *International Journal of Heat and Mass Transfer*, vol. 43, pp. 2089-2099, 2000.

[13] S. Mahmud and R. A. Fraser, Magnetohydrodynamic free convection and entropy generation in a square porous cavity, *International Journal of Heat and Mass Transfer*, vol. 47, pp. 3245-3256, 2004.

[14] G. Ovando-Chacon, S. Ovando-Chacon, and J. Prince-Avelino, Entropy generation due to mixed convection in an enclosure with heated corners, *International Journal of Heat and Mass Transfer*, vol. 55, pp. 695-700, 2012.

[15] H. Khorasanizadeh, M. Nikfar, and J. Amani, Entropy generation of Cu–water nanofluid mixed convection in a cavity, *European Journal of Mechanics-B/Fluids*, vol. 37, pp. 143-152, 2013.

[16] R. Nayak, S. Bhattacharyya, and I. Pop, Numerical study on mixed convection and entropy generation of a nanofluid in a lid-driven square enclosure, *Journal of Heat Transfer*, vol. 138, p. 012503, 2016.

[17] A. Aghaei, H. Khorasanizadeh, G. Sheikhzadeh, and M. Abbaszadeh, Numerical study of magnetic field on mixed convection and entropy generation of nanofluid in a trapezoidal enclosure, *Journal of Magnetism and Magnetic Materials*, vol. 403, pp. 133-145, 2016.

[18] C. Beghein, F. Haghighat, and F. Allard, Numerical study of double-diffusive natural convection in a square cavity, *International Journal of Heat and Mass Transfer*, vol. 35, pp. 833-846, 1992.

[19] K. Ghorayeb and A. Mojtabi, Double diffusive convection in a vertical rectangular cavity, *Physics of Fluids*, vol. 9, pp. 2339-2348, 1997.

[20] M. A. Teamah, Double-diffusive laminar natural convection in a symmetrical trapezoidal enclosure, *Alexandria Engineering Journal*, vol. 45, pp. 251-263, 2006.

[21] M. Corcione, S. Grignaffini, and A. Quintino, Correlations for the double-diffusive natural convection in square enclosures induced by opposite temperature and concentration gradients, *International Journal of Heat and Mass Transfer*, vol. 81, pp. 811-819, 2015.

[22] M. Nazari, L. Louhghalam, and M. H. Kayhani, Lattice Boltzmann simulation of double diffusive natural convection in a square cavity with a hot square obstacle, *Chinese Journal of Chemical Engineering,* vol. 23, pp. 22-30, 2015.

[23] G. Swapna, L. Kumar, P. Rana, A. Kumari, and B. Singh, Finite element study of radiative double-diffusive mixed convection magneto-micropolar flow in a porous medium with chemical reaction and convective condition, *Alexandria Engineering Journal*, 2017.

[24] A. A. Abbasian Arani, A. Ababaei, G. A. Sheikhzadeh, and A. Aghaei, Numerical simulation of double-diffusive mixed convection in an enclosure filled with nanofluid using Bejan's heatlines and masslines, *Alexandria Engineering Journal*, 2017.

[25] A. Bejan, Combined Heat and lass Transfer by Natural Convection in a Vertical Enclosure, 1987.

[26] V. Costa, Double diffusive natural convection in a square enclosure with heat and mass diffusive walls, *International Journal of Heat and Mass Transfer,* vol. 40, pp. 4061-4071, 1997.

[27] A. M. Al-Amiri, K. M. Khanafer, and I. Pop, Numerical simulation of combined thermal and mass transport in a square lid-driven cavity, *International journal of thermal sciences,* vol. 46, pp. 662-671, 2007.

[28] M. Hasanuzzaman, M. Rahman, H. F. Öztop, N. Rahim, and R. Saidur, Effects of Lewis number on heat and mass transfer in a triangular cavity, *International Communications in Heat and Mass Transfer*, vol. 39, pp. 1213-1219, 2012.

[29] F. Oueslati, B. Ben-Beya, and T. Lili, Double-diffusive natural convection and entropy generation in an enclosure of aspect ratio 4 with partial vertical heating and salting sources, *Alexandria Engineering Journal*, vol. 52, pp. 605-625, 2013.

[30] Q. Qin, Z. Xia, and Z. F. Tian, High accuracy numerical investigation of double-diffusive convection in a rectangular enclosure with horizontal temperature and concentration gradients, *International Journal of Heat and Mass Transfer,* vol. 71, pp. 405-423, 2014.

[31] N. Arbin, H. Saleh, I. Hashim, and A. Chamkha, Numerical investigation of double-diffusive convection in an open cavity with partially heated wall via heatline approach, *International Journal of Thermal Sciences,* vol. 100, pp. 169-184, 2016.

[32] M. A. Teamah and A. I. Shehata, Magnetohydrodynamic double diffusive natural convection in trapezoidal cavities, *Alexandria Engineering Journal*, vol. 55, pp. 1037-1046, 2016.

[33] S. Kimura and A. Bejan, The "heatline" visualization of convective heat transfer, *Journal of heat transfer*, vol. 105, pp. 916-919, 1983.

[34] V. Costa, Bejan's heatlines and masslines for convection visualization and analysis, *Applied Mechanics Reviews*, vol. 59, pp. 126-145, 2006.

[35] P. Biswal and T. Basak, Bejan's heatlines and numerical visualization of convective heat flow in differentially heated enclosures with concave/convex side walls, *Energy*, vol. 64, pp. 69-94, 2014.

[36] P. Biswal and T. Basak, Sensitivity of heatfunction boundary conditions on invariance of Bejan's heatlines for natural convection in enclosures with various wall heatings, *International Journal of Heat and Mass Transfer*, vol. 89, pp. 1342-1368, 2015.

[37] M. Rahman, H. F. Öztop, S. Mekhilef, R. Saidur, and J. Orfi, Simulation of unsteady heat and mass transport with heatline and massline in a partially heated open cavity, *Applied Mathematical Modelling*, vol. 39, pp. 1597-1615, 2015.

[38] A. Alsabery, A. Chamkha, S. Hussain, H. Saleh, and I. Hashim, Heatline visualization of natural convection in a trapezoidal cavity partly filled with nanofluid porous layer and partly with non-Newtonian fluid layer, *Advanced Powder Technology*, vol. 26, pp. 1230-1244, 2015.

[39] H. F. Oztop and K. Al-Salem, A review on entropy generation in natural and mixed convection heat transfer for energy systems, *Renewable and Sustainable Energy Reviews*, vol. 16, pp. 911-920, 2012.

[40] M. Magherbi, H. Abbassi, N. Hidouri, and A. B. Brahim, Second law analysis in convective heat and mass transfer, *Entropy*, vol. 8, pp. 1-17, 2006.

[41] K. Ghachem, L. Kolsi, C. Mâatki, A. K. Hussein, and M. N. Borjini, Numerical simulation of three-dimensional double diffusive free convection flow and irreversibility studies in a solar distiller, *International Communications in Heat and Mass Transfer*, vol. 39, pp. 869-876, 2012.

[42] F.-Y. Zhao, D. Liu, and G.-F. Tang, Application issues of the streamline, heatline and massline for conjugate heat and mass transfer, *International Journal of Heat and Mass Transfer,* vol. 50, pp. 320-334, 2007.

[43] H. K. Versteeg and W. Malalasekera, *An introduction to computational fluid dynamics: the finite volume method*: Pearson Education, 2007.

[44] S. V. Patankar, Numerical heat transfer and fluid flow,(1980), *Hemisphere, New York,* pp. 25-73, 1980.

[45] G. G. Ilis, M. Mobedi, and B. Sunden, Effect of aspect ratio on entropy generation in a rectangular cavity with differentially heated vertical walls, *International Communications in Heat and Mass Transfer,* vol. 35, pp. 696-703, 2008.

Table 1. The average Nusselt and Sherwood number, and total entropy generation in Ri = 0.01, Le = 10, Br = 10, and $\gamma = 45°$ for different grid sizes

Grid size	Nu_{av}	Sh_{av}	$\dot{S}$	Max. Rel. Diff.
51×25	9.0613	18.5992	10.6140	-
101×51	10.6015	23.3730	11.5842	25.67
201×101	11.1811	26.0227	12.1350	11.34
301×151	11.3495	26.4604	12.1892	1.68

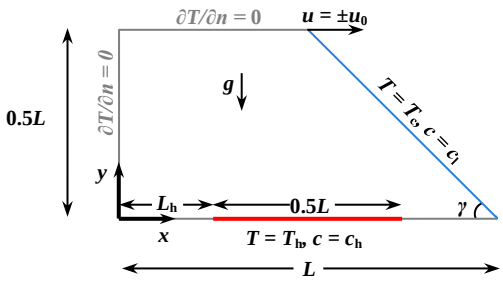

Fig. 1. Schematic of the problem

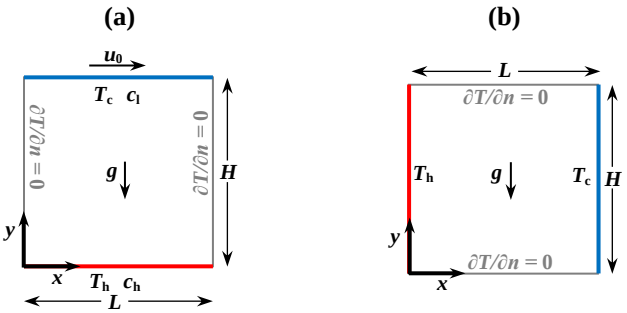

Fig. 2. Domain and boundary conditions of

(a) Al-Amiri et al. [27] study; and **(b)** Ilis et al. [45] study

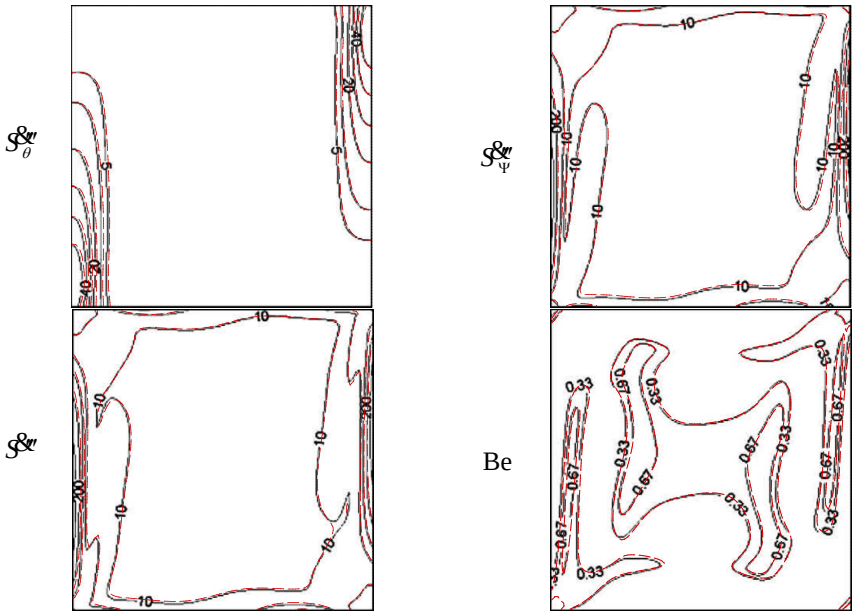

Fig. 3. Comparisons between the heat transfer and fluid friction irreversibilities, the total rate of entropy generation, and the local Bejan number of the present study code (– –) with the results of Ilis et al. [45] for Pr = 0.7 for Ra = 10^5

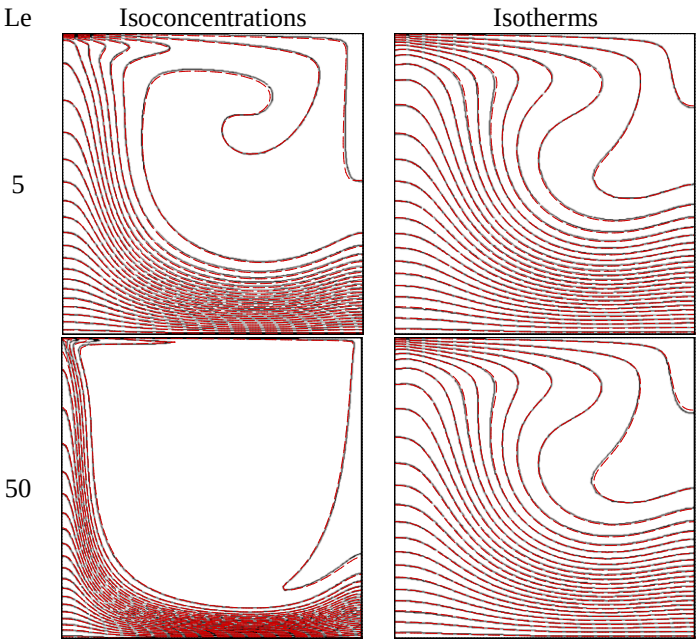

Fig. 4. Comparisons between the isoconcentration lines and isotherms of the simulated results of Al-Amiri et al. [27] with those of the present study code (– –) for Pr = 1, Ri = 0.01, Re = 100, Br = 1, and Le = 5 and 50

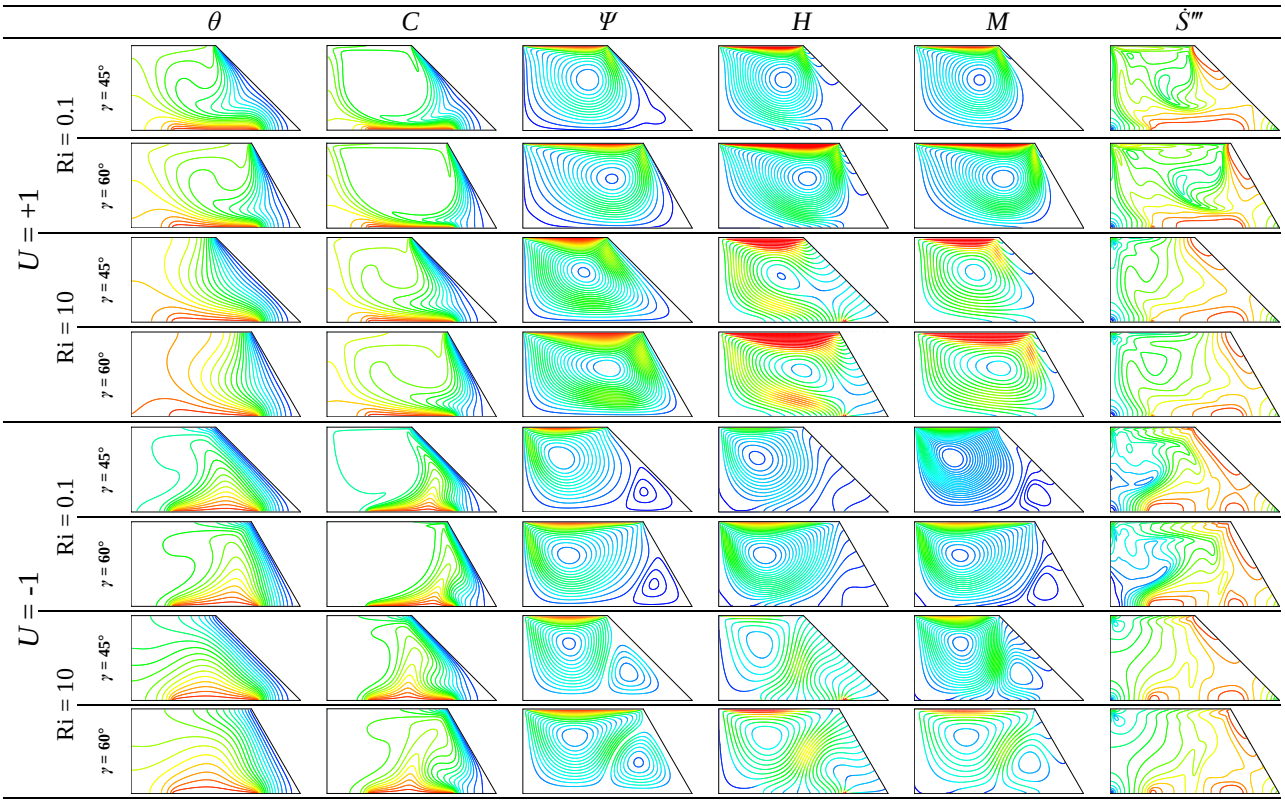

Fig. 5. Isotherms, isoconcentration lines, streamlines, heatlines, masslines, and constant generated entropy lines for Le = 10, Br = 1, Ri = 0.1 and 10, γ = 45° and 60° for two directions of lid movement

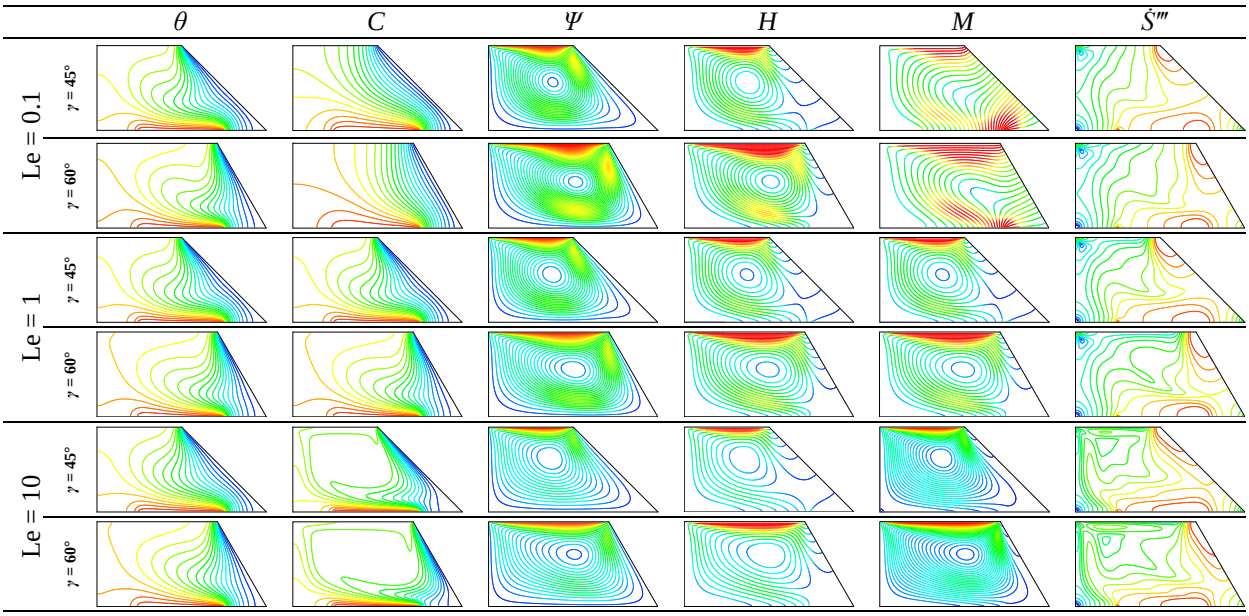

Fig. 6. Isotherms, isoconcentration lines, streamlines, heatlines, masslines, and constant generated entropy lines for Ri = 1, Br = 4, and γ = 45° and 60° for different Lewis numbers

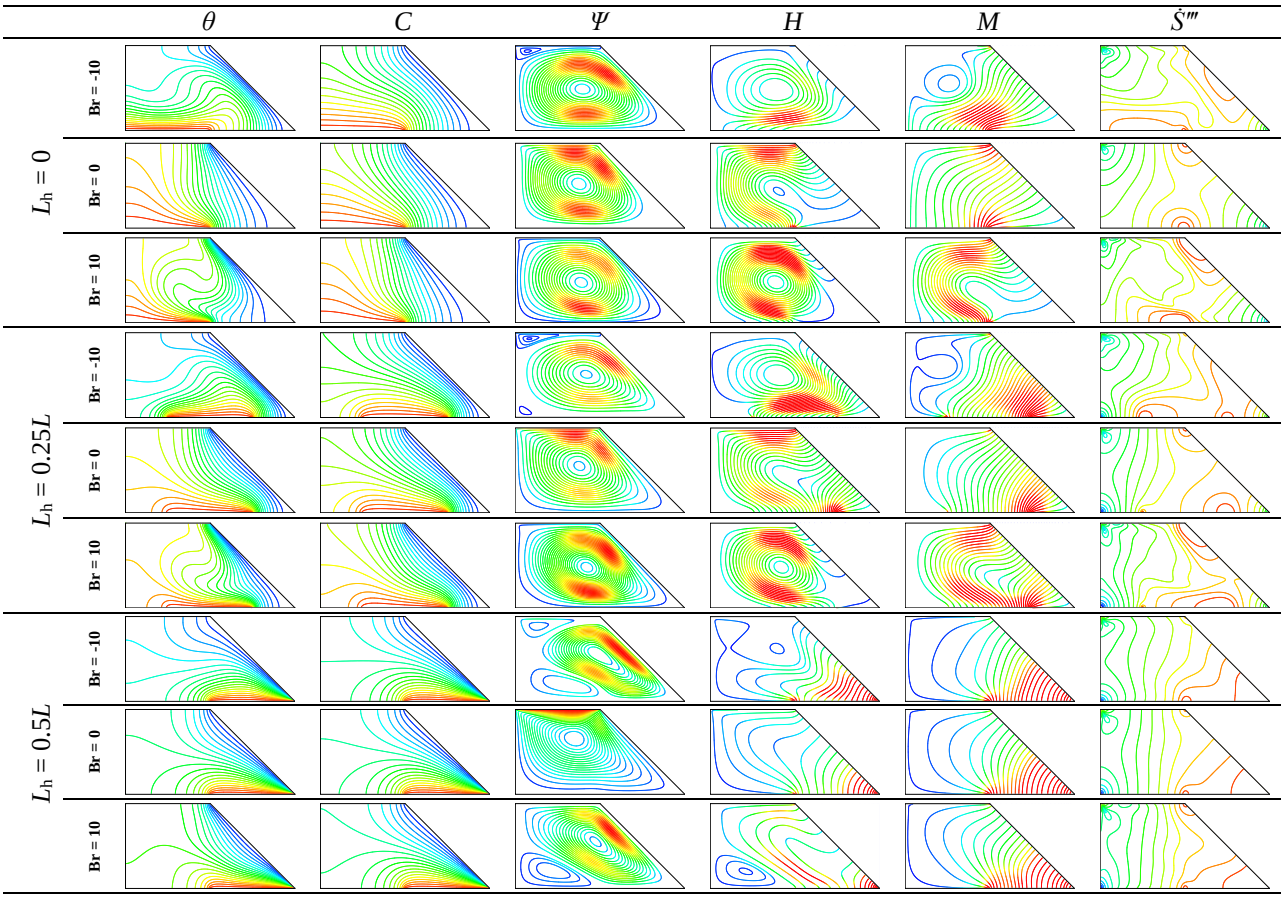

Fig. 7. Isotherms, isoconcentrations, streamlines, heatlines, masslines, and constant generated entropy lines for Ri = 100, Le = 0.1, γ = 45° for different buoyancy ratios and heat source places

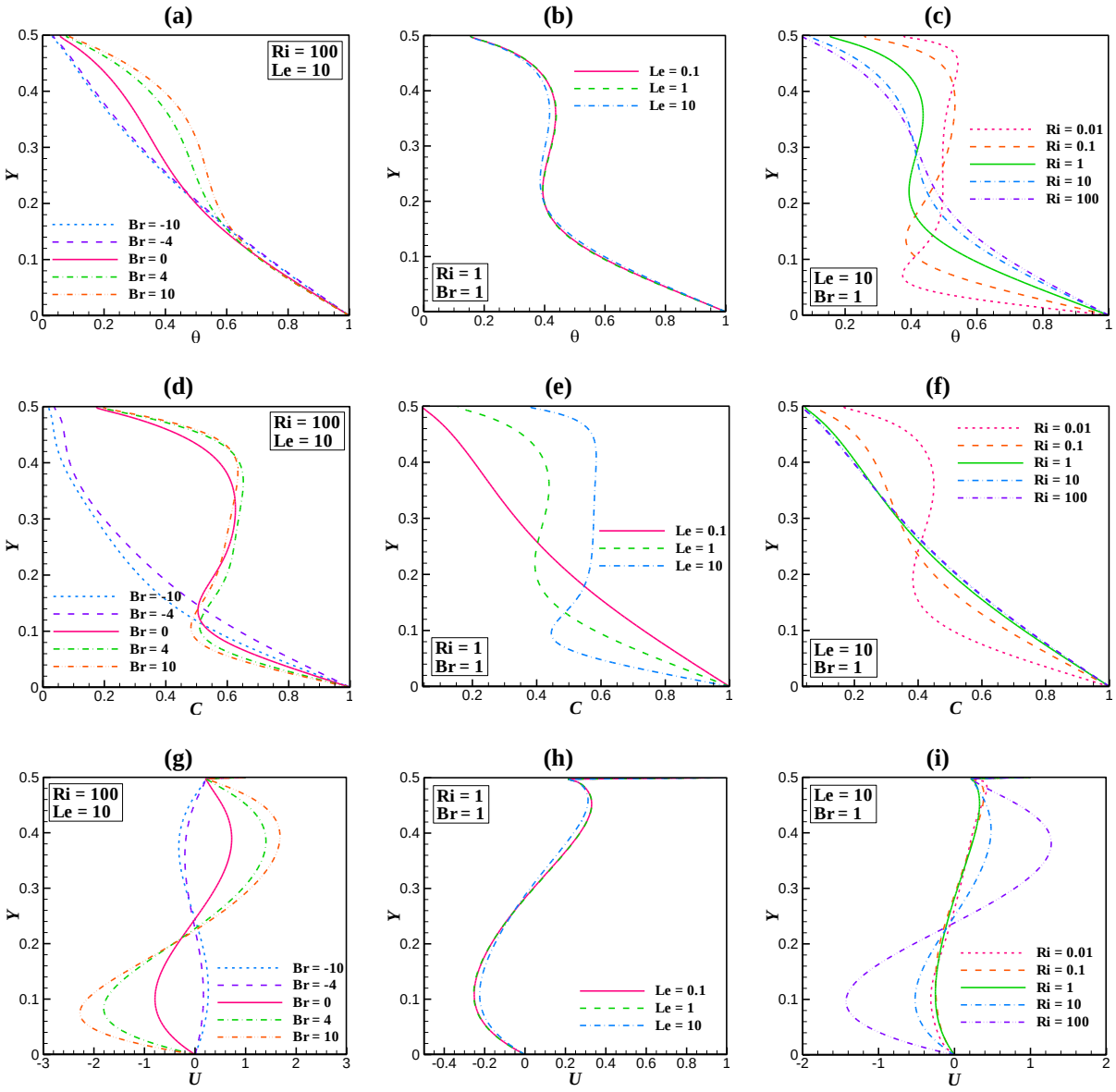

Fig. 8. Variations of the dimensionless temperature, the concentration, and the velocity along vertical centerline of the enclosure for $\gamma = 45°$ for different buoyancy ratios and Lewis and Richardson numbers

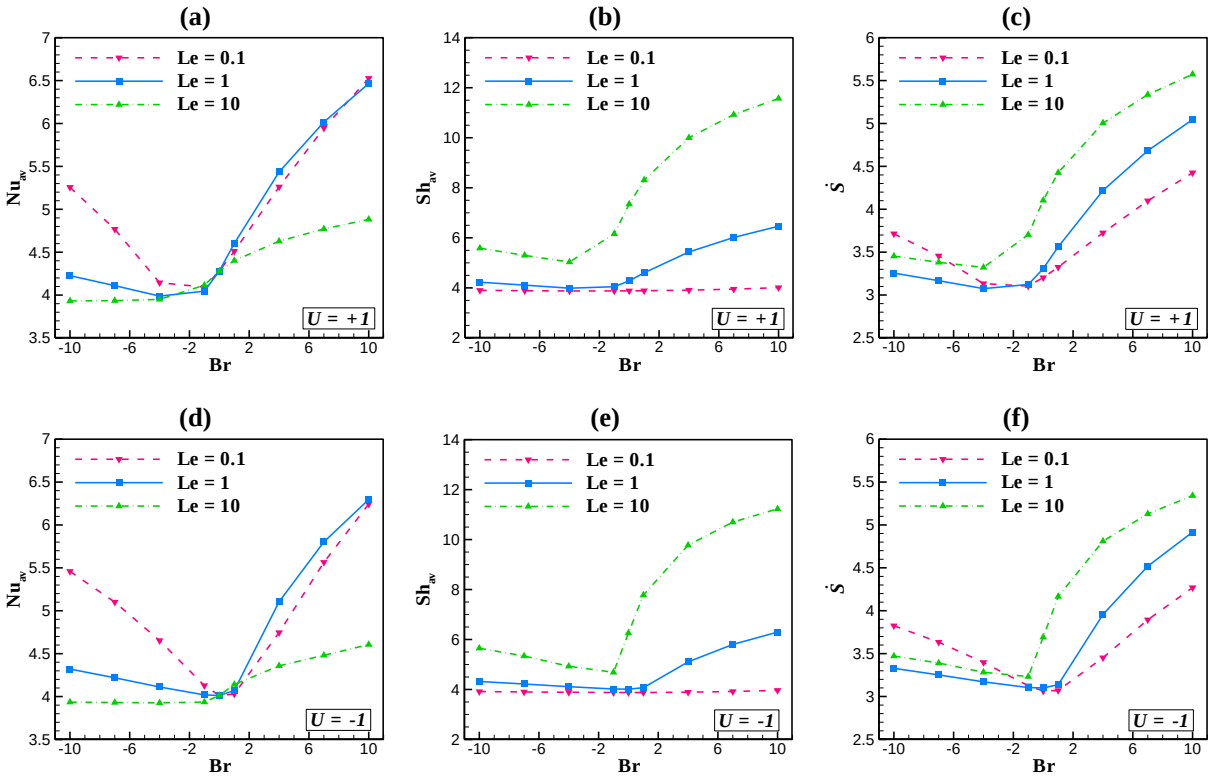

Fig. 9. Variations of the mean Nusselt and Sherwood numbers and total entropy generation with buoyancy ratio in Ri = 10 and γ = 45° for different Lewis numbers and two directions of lid movement

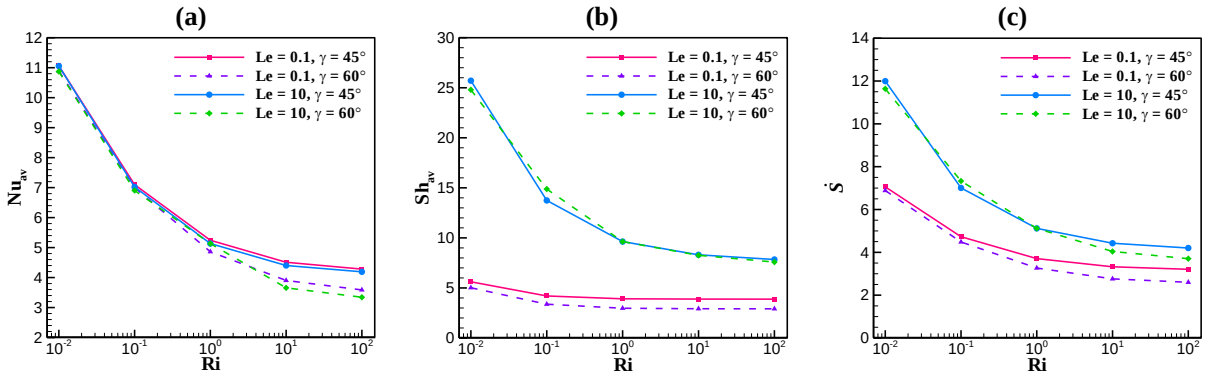

Fig. 10. Variations of the mean Nusselt and Sherwood numbers and the total entropy generation with Richardson number for Br = 1, Le = 0.1 and 10, and γ = 45° and 60°

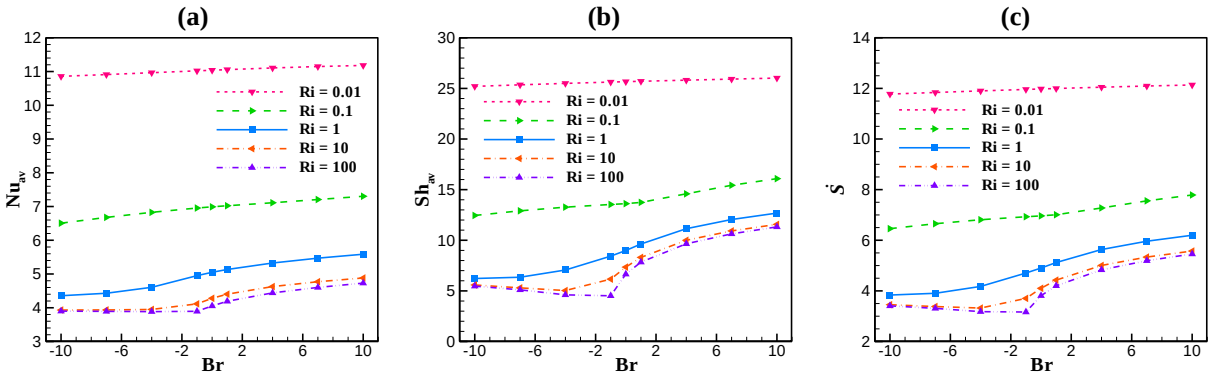

Fig. 11. Variations of the mean Nusselt and Sherwood numbers and the total entropy generation with buoyancy ratio for Le = 10 and γ = 45° for different Richardson numbers

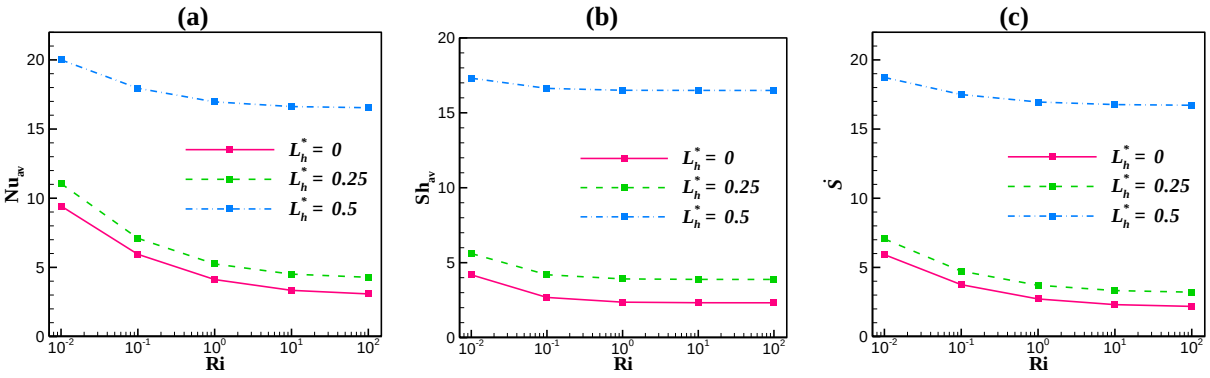

Fig. 12. Variations of the mean Nusselt and Sherwood numbers and the total entropy generation with Richardson number for Br = 1, Le = 0.1, and $\gamma = 45°$ for different heat source locations on bottom wall